Intrinsic Stability of a Body Hovering in an Oscillating Airflow

Bin Liu, Leif Ristroph, Annie Weathers, Stephen Childress, and Jun Zhang

Phys. Rev. Lett. **108**, 068103 — Published 9 February 2012

DOI: 10.1103/PhysRevLett.108.068103

Intrinsic stability of a body hovering in an oscillating airflow

Bin Liu[1], Leif Ristroph[1], Annie Weathers[1], Stephen Childress[1], and Jun Zhang[1,2]
[1]*Applied Mathematics Laboratory, Courant Institute, New York University, 251 Mercer Street, New York, NY 10012 and*
[2]*Department of Physics, New York University, 4 Washington Place, New York, NY 10003*

We explore the stability of flapping flight in a model system that consists of a pyramid-shaped object hovering in a vertically oscillating airflow. Such a flyer not only generates sufficient aerodynamic force to keep aloft but also robustly maintains balance during free flight. Flow visualization reveals that both weight support and orientational stability result from the periodic shedding of vortices. We explain these findings with a model of the flight dynamics, predict increasing stability for higher center-of-mass, and verify this counterintuitive fact by comparing top- and bottom-heavy flyers.

While airplane flight relies on the force generated by a steadily translating airfoil, insect flight is driven by flapping wing motions. This unsteady flow-structure interaction offers mechanisms of force generation that are not described by fixed-wing aerodynamics [1–4]. Experimental [5–7] and theoretical [8–11] studies have revealed the importance of vortices as a signature of unsteady mechanisms. For example, the attachment of a leading-edge vortex enhances lift on the wings of some insects [5, 6], and vortex shedding indicates force production in others [9]. The role of unsteady effects in flapping flight stability is less explored. Insects certainly employ active feedback control during flight [12, 13], although it is unclear if such systems are indispensable. Some simulations of insect flight indicate that body orientation is intrinsically unstable [14, 15] while others predict neutral stability [16] and even passive stability [17]. Unfortunately, experiments that directly assess the intrinsic stability of insects are difficult or perhaps impossible to perform.

As an alternative approach, we consider an inanimate flyer that shares important features with its biological counterpart but is amenable to a rigorous stability analysis. Our model flapping flight system consists of upward-pointing pyramid-shaped objects, or 'bugs', made to hover in a vertically oscillating column of air [18, 19]. Tethered flight experiments have shown that the interaction between this asymmetric shape and reciprocal flow results in an upward force capable of supporting body weight [19]. Qualitatively, the force can be understood in terms of differential drag, with the upward flow inducing greater drag than the downward flow. Quantitatively, however, the force produced defies such an accounting by quasi-steady aerodynamics, and thus unsteady flow effects are critical to force generation. In this work, we observe the unrestricted hovering of such bugs, thus enabling a direct assessment of free flight stability. In addition, we use flow visualization to reveal the importance of unsteady aerodynamic effects in both force generation and flight stabilization. The mechanisms discerned here are in principle available in other modes of flapping flight.

Our system consists of a low-frequency loudspeaker ('subwoofer') that is directed upwards, capped, and fitted with a clear test section of 15 cm in both diameter and height. The speaker is driven with a signal generator and amplifier to produce a sinusoidal vertical airflow of tunable frequency and amplitude, typically $f = 10 - 50$ Hz and $A = 1 - 5$ cm (peak-to-peak). Previous work has shown that this chamber produces high-quality laminar flow [18, 19]. We examine the free flight of hollow pyramid-shaped bugs of height $L = 1 - 5$ cm and mass 0.1-0.5 g constructed from either letter paper or tissue paper with carbon fiber supports. The Reynolds number is typically $\mathrm{Re} = fAL/\nu \sim 10^3$, where $\nu = 1.5 \times 10^{-5}$ m^2/s is the kinematic viscosity of air.

For sufficiently high frequency and amplitude, a bug hovers with its apex pointing up and also displays remarkably robust stability. In Fig. 1(a), we overlay snapshots captured from high-speed video of a bug in hovering flight. While aloft, it is often tilted to the side but quickly recovers the upright orientation. Flight can last as long as thousands of oscillation periods, eventually ending in a collision with the chamber walls. From many videos, we extract the pyramid's tilt angle θ, and sample trajectories are shown in Fig. 1(b). The angle is defined with respect to the vertical and thus is always non-negative with $\theta = 0$ corresponding to the upright orientation. The pyramid occasionally experiences large excursions, $\theta > 30$ degrees, but reliably recovers. Our observation of such long-lived flight for pyramids and also cones of various opening angles and sizes suggests that body orientation is generically stable.

To quantify these observations, we formulate an aerodynamic potential that describes the bug's orientational stability. From measurements of θ, we determine the angular acceleration and thus the net torque $\Gamma \propto \ddot{\theta}$ on the body. Because the gravitational force acts through the center-of-mass and thus generates no torque, Γ reflects only aerodynamic effects. Using $V(\theta) = -\int_0^\theta \Gamma(\theta')\mathrm{d}\theta'$, we determine the potential from 16 videos, as shown by the gray points in Fig. 1(c). For small angles, this potential is essentially flat and thus corresponds to near neutral stability. It rises sharply for larger angles, however, revealing that the bug hovers in a potential well that resists excursions to large angles.

To elucidate the fluid mechanical basis of this stability, we investigate an analogous two-dimensional system. A Λ-shaped body is fixed in a pan containing a shallow (2 cm) layer of water, and a motor tilts the pan back-

and-forth about a pivot to produce an oscillating flow. The body size of 3 cm and flow period of 1 s ensure that Re $\sim 10^3$. A shadowgraph technique is used to visualize the deformations of the fluid surface, revealing flows of strong vorticity [20]. When upright, each side of the body sheds a vortex dipole once per oscillation. As shown in Fig. 2(a), the outer vortex of each pair is formed as the upward flow curls around the body, and the inner vortex forms during the downward flow. The two counter-rotating vortices then shed as a pair, forming a strong downwash [Fig. 2(b)]. This downward transport of fluid momentum is associated with an upward reaction force on the body itself [21]. Similarly, for a three-dimensional pyramid, we expect that counter-rotating vortex tubes first envelope the base and are then ejected downward.

When the Λ-shaped body is tilted, a strong asymmetry appears in the surrounding flow field. As shown in Fig. 2(c) and (d) for a rightward tilt, a downward-moving vortex dipole is again produced on the right side of the body, but the dipole produced on the left side is ejected sideways. In this case, the leftward transport of fluid momentum corresponds to a rightward force. Because the line-of-action of this force is below the center-of-mass, it produces a torque that tends to restore the body to the upright orientation. Indeed, if free to rotate, the body tends to align with the flow.

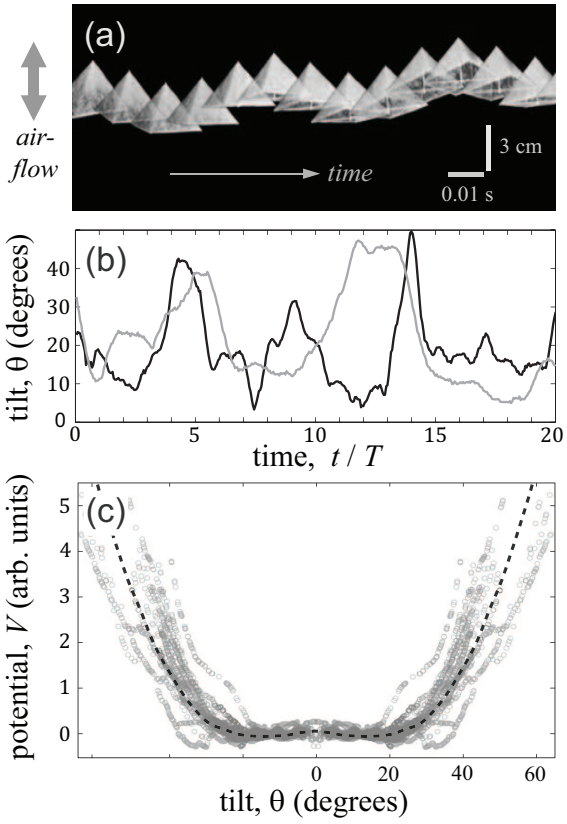

FIG. 1: Stable hovering of a pyramid in an oscillating airflow. (a) Snapshots from high-speed video of free flight of a paper pyramid (mass 0.22 g and height $L = 3.2$ cm). The flow oscillates up-and-down with peak-to-peak amplitude $A = 1.9$ cm and frequency $f = 20$ Hz (period $T = 0.05$ s). (b) Typical traces of the body tilt angle θ, which is measured from the vertical. (c) An aerodynamic potential is reconstructed from the tilt dynamics of 16 movies (gray points), and data for $\theta \geq 0$ is reflected about the vertical to reveal a stable potential well (dashed line).

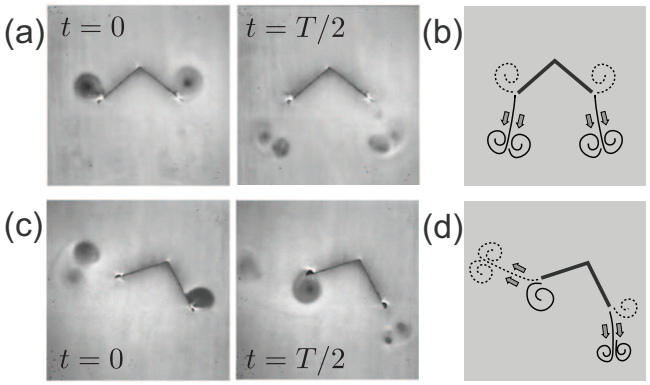

FIG. 2: Vortex ejection for a Λ-shaped body in an oscillating flow. A water-filled pan is rocked back-and-forth, and flow structures are visualized with shadowgraphs. (a) Snapshots of the flow around an upright Λ. A vortex curls around each side of the body as the flow moves upwards ($t = 0$), a counter-rotating vortex then forms on the downward flow, and the pair are shed downward ($t = T/2$). (b) Schematic of the flow field for an upright body. (c) and (d) When tilted rightward, the left side emits a pair outward and nearly perpendicular to the body axis ($t = 0$), and the right side of the body emits a weaker vortex pair downward ($t = T/2$).

These flow observations inspire a two-dimensional model in which the average fluid forces act at the sites of vortex emission. Further, to employ symmetry arguments, we idealize the Λ-shape as an equilateral triangle with all three sides closed to the flow. First, we consider forces on the left side of the body, which is made to protrude into the flow under a rightward rotation, as shown in Fig. 3(a). When upright, the force points upward and supports half of the body weight. For $\theta = 60$ degrees, the configuration is the up-down mirror-symmetric partner of $\theta = 0$ and thus the force must now point downward. Thus, as θ sweeps from 0 to 60 degrees, the force vector sweeps from 0 to 180 degrees. This suggests that for intermediate values of θ the angle of the force vector is about three times the body tilt, as is consistent with the strong re-direction of vortex emission seen in experiments [Fig. 2(c) and (d)]. Assuming a constant force magnitude leads to the entire sequence given in Fig. 3(a).

We use similar arguments for the force on the right side of the body, as shown by the sequence of Fig. 3(b). For a tilted body, flow visualization reveals that weaker vortices are shed downward [Fig. 2(c) and (d)]. Thus, for $\theta < 30$, we assume the force vector remains pointing upward but its strength decreases linearly in θ. For tilts $30 < \theta < 60$, symmetry requires that the force vector now act on the upper corner, point downward, and increase

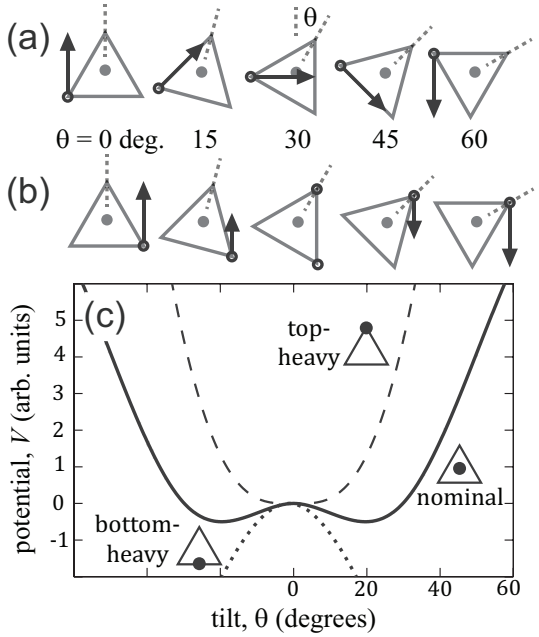

FIG. 3: A point-force model of stability. Time-averaged aerodynamic forces (dark arrows) on a triangular body are assumed to act at the sites of vortex emission. (a) As the body tilts, the force vector on the left side maintains constant magnitude, and its angle is three times the tilt angle θ. (b) The force on the right points upward and decreases in strength as θ increases to 30 degrees. Similarly, it is directed downward and grows in strength for $30 < \theta < 60$. (c) Potential for the nominal case in which the center-of-mass is midway between the apex and base, as well as for top-heavy (dashed) and bottom-heavy (dotted) arrangements.

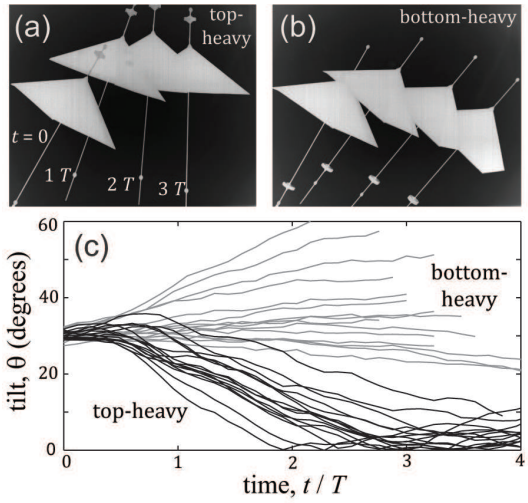

FIG. 4: Center-of-mass (CoM) location and flight stability. Weights are added to the pyramid to make top- and bottom-heavy bodies. The pyramid height is 1.7 cm in both cases, and the CoM is located at the apex and 1.5 cm below the base, respectively. The objects are released into the flow with tilt $\theta = 30$ degrees. (a) and (b) A top-heavy pyramid recovers the upright orientation, while a bottom-heavy body tips over. (c) Body tilt dynamics for top- and bottom-heavy pyramids.

in strength for larger tilts.

With the specification of the center-of-mass (CoM) location, the model is complete and contains no adjustable parameters. For the nominal case of a Λ-shape – with mass on the two sides but not on the bottom – the CoM is located halfway between its apex and base. For all angles θ, we sum the torques about this CoM and integrate the net torque to form the potential. As shown in Fig. 3(c), this theoretical potential is surprisingly similar to that measured for a three-dimensional pyramid [Fig. 1(c)]. The model accounts for the passive stability and captures such features as the rapid increase in the potential for $\theta > 30$ degrees and even the slight negative stability near $\theta = 0$.

In addition, the model indicates that intrinsic stability depends on being top-heavy. In particular, if the CoM is located higher, say at the apex, the potential walls become tighter and steeper, further increasing stability [dashed line of Fig 3(c)]. If, on the other hand, the CoM is lowered to the base of the body, flight becomes unstable, as shown by the dotted potential of Fig. 3(c). This prediction of increasing stability for top-heavy bodies defies conventional wisdom but can be rationalized by considering the force diagrams of Fig. 3(a): the inward force leads to a restorative torque only if the body's CoM is located above the line-of-action.

To test this prediction, we compare the flight of top- and bottom-heavy pyramids. The CoM is shifted by attaching a metal weight to a thin rod that runs through the axis of the body. These bugs are then released into the flow from a tilted initial orientation, and the resulting dynamics offer a clear view of the stability characteristics. Top-heavy bugs consistently return to the upright orientation when released, as exemplified by the snapshots of Fig. 4(a). In Fig, 4(c), we plot in black the time-course of the tilt angle for many such trials and find that the body orientation experiences decaying oscillations. Bottom-heavy bugs, on the other hand, often flip over when released, as shown in Fig. 4(b). The associated trajectories show a divergence toward large tilt angles [gray curves of Fig. 4(c)], and thus balance is lost by lowering the CoM.

These findings show how unsteady aerodynamics and CoM location lead to surprising features of flapping flight stability. Typically, flight stability can only be ensured through careful distribution of weight and lifting surfaces [22, 23]. In our system, on the other hand, the simplest up-down asymmetric shapes that are able to produce lift also lead to stability. The key element is the sensitive dependence of the angle of vortex emission on the orientation of the body, and future studies that include computational simulations will likely provide additional insights into the role of such unsteady flow effects.

More broadly, expressing the relevant physical factors as dimensionless quantities offers general insights

into hovering. A dimensional analysis of our system reveals seven groups of variables whose values characterize force generation and stability. Vortex shedding demands that fluid inertia overcome viscosity and thus that the Reynolds number be high, $\mathrm{Re} \gg 1$. Weight support also requires that the flow acceleration be comparable to gravitational acceleration, $Af^2/g \sim 1$. Force production has been found to be most effective when the flow amplitude and body size are comparable, $A/L \sim 1$ [18]. Likewise, a strong asymmetry is needed, which is associated with a pyramid opening angle of about 60 degrees [19]. For free flight, three additional parameters are introduced that relate to the body mass, moment of inertia, and CoM location. The large body-to-fluid mass ratio ($m/\rho L^3 \sim 10$, where ρ is the fluid density) indicates that flyers must rely on aerodynamic forces and not buoyancy. The moment of inertia ($I/\rho L^5 \sim 10$) does not affect the fluid torque nor the potential but alters only the time-scales of the dynamics, as shown below. Finally, as we emphasize here, the CoM height above the base ($h/L \sim 0.1-1$) is a critical determinant of stability.

Estimates for important quantities can be expressed in terms of these parameters. The high-Re fluid force relative to body weight can be estimated as $\rho(Af)^2L^2/mg = (\rho L^3/m)(Af^2/g)(A/L) \sim 0.1$. This ratio must be unity for hovering, of course, and the underestimate reflects the deficiency of quasi-steady calculations [19]. For stability, recovery from a tilt is determined by fluid torques ($\sim mgh$) overcoming body inertia, which for our system yields a dimensionless recovery time of $\sqrt{I/mgh}/T = \sqrt{(I/\rho L^5)(\rho L^3/m)(Af^2/g)(L/A)(L/h)} \sim 1$. Thus, stabilization occurs as fast as an oscillation, as is consistent with the dynamics of Figs. 1(b) and 4(c).

While we know of no insect that employs the particular flight strategy studied here – by, say, symmetrically heaving an asymmetric wing – the shedding of dipolar vortices is a critical feature common to our system and insects [9]. Our results suggest that future studies might evaluate how this shedding process is modified when an insect experiences an in-flight perturbation [13]. Understanding such unsteady flow mechanisms may help resolve the current disagreement among models that assess the intrinsic stability of insects. Further, a complete analysis of insect flight stability will require knowledge of the CoM location and, in particular, the spatial arrangement and time-variation of fluid forces relative to this point.

Finally, the potential revealed here may be ideal for a free-flying device. In addition to the potential well, the region of neutral stability would not hinder the intentional reorientation needed for maneuvering. Thus this arrangement offers a simultaneous realization of the desirable but antagonistic goals of stability and maneuverability. A robot inspired by this work – for example, a pyramid or cone driven to flap up-and-down – would represent an alternative approach to the more literal biomimetic implementations that flap wings in a manner similar to insects [24, 25]. The lack of a direct biological analog for our conceptual vehicle does not necessarily imply an inferior design, but perhaps one that has not yet been explored by evolution.

We thank M. Shelley, A. Libchaber, and N. Moore for helpful discussions and the DOE (DE-FG02-88ER25053) and NSF (DMS-0507615, MRI-0821520, and DMS-1103876) for support.

[1] R. Dudley, *The Biomechanics of Insect Flight* (Princeton University Press, Princeton, 2000).
[2] S. P. Sane, J. Exp. Biol. **206**, 4191 (2003).
[3] F.-O. Lehmann, Naturwissenschaften **91**, 101 (2004).
[4] Z. J. Wang, Annu. Rev. Fluid Mech. **37**, 183 (2005).
[5] C. P. Ellington, C. van den Berg, A. P. Willmott, and A. L. R. Thomas, Nature **384**, 626 (1996).
[6] M. H. Dickinson, F.-O. Lehmann, and S. P. Sane, Science **284**, 1954 (1999).
[7] N. Vandenberghe, J. Zhang, and S. Childress, J. Fluid Mech. **506**, 147 (2004).
[8] C. P. Ellington, Phil. Trans. R. Soc. Lond. B **305**, 79 (1984).
[9] Z. J. Wang, Phys. Rev. Lett. **85**, 2216 (2000).
[10] R. Ramamurti and W. C. Sandberg, J. Exp. Biol. **205**, 1507 (2002).
[11] S. Alben and M. Shelley, PNAS **102**, 11163 (2005).
[12] G. K. Taylor and H. G. Krapp, Adv. Insect. Physiol. **34**, 231 (2007).
[13] L. Ristroph, A. J. Bergou, G. Ristroph, K. Coumes, G. J. Berman, J. Guckenheimer, Z. J. Wang, and I. Cohen, PNAS **107**, 4820 (2010).
[14] M. Sun and Y. Xiong, J. Exp. Biol. **208**, 447459 (2005).
[15] I. Faruque and J. S. Humbert, J. Theor. Biol. **264**, 538 (2010).
[16] G. K. Taylor and A. L. R. Thomas, J. Theor. Biol. **214**, 351 (2002).
[17] N. Gao, H. Aono, and H. Liu, J. Biomech. Sci. Eng. **4**, 105 (2009).
[18] S. Childress, N. Vandenberghe, and J. Zhang, Phys. Fluids **18**, 117103 (2006).
[19] A. Weathers, B. Folie, B. Liu, S. Childress, and J. Zhang, J. Fluid Mech. **650**, 415 (2010).
[20] G. S. Settles, *Schlieren and shadowgraph techniques: Visualizing phenomena in transparent media* (Springer-Verlag, Berlin, 2001).
[21] G. K. Batchelor, *An Introduction to Fluid Dynamics* (Cambridge University Press, Cambridge, 2000).
[22] M. J. Abzug and E. E. Larrabee, *Airplane Stability and Control: A History of the Technologies That Made Aviation Possible* (Cambridge University Press, Cambridge UK, 2002).
[23] R. F. Stengel, *Flight dynamics* (Princeton University Press, Princeton, 2004).
[24] F. van Breugel, W. Regan, and H. Lipson, IEEE Robotics and Automation Magazine **15**, 68 (2008).
[25] R. J. Wood, IEEE Trans. on Robotics **24**, 341 (2008).